FFSiOH: a New Force Field for Silica Polymorphs and Their Hydroxylated Surfaces Based on Periodic B3LYP Calculations

Alfonso Pedone,[†] Gianluca Malavasi,[†] M. Cristina Menziani,[†] Ulderico Segre,[†] Federico Musso,[‡] Marta Corno,[‡] Bartolomeo Civalleri,[‡] and Piero Ugliengo*,[‡]

Department of Chemistry and SCS center, University of Modena and Reggio Emilia, Via G. Campi 183, 41100 Modena, Italy, and Department of Chemistry IFM, NIS Centre of Excellence and INSTM (Materials Science and Technology) National Consortium, University of Torino, Via P. Giuria 7, Torino, Italy

Received December 4, 2007. Revised Manuscript Received January 16, 2008

A partial charge shell-ion model potential for silica polymorphs and their hydroxylated surfaces (FFSiOH) was parametrized in a self-consistent way using periodic B3LYP results for bulk α-cristobalite and the (100) and (001) hydroxylated surfaces. The reliability of the new potentials was checked by comparing structures, vibrational frequencies and relative phase stabilities of dense bulk silica polymorphs, namely α-quartz, α-cristobalite, α-tridymite, and Stishovite with both experimental and B3LYP data. The FFSiOH was also checked for computing structural and vibrational features of representative all-silica microporous materials, namely edingtonite, chabazite, and faujasite. As a last step, FFSiOH was adopted to predict OH stretching vibrational frequencies and relative thermodynamic stability of the most common fully hydroxylated surfaces of the dense silica polymorphs, the (100) and (001) faces of all-silica edingtonite, the features of the local Si-defect in chabazite and sodalite known as $(SiOH)_4$ hydrogarnet and the geometries of H-bonded silanol groups of an amorphous silica surface. In all cases excellent agreement resulted between FFSiOH and B3LYP periodic data and experimental data, when available. The new FFSiOH force field opens up the molecular simulation of materials in which the surface hydroxyl groups play a key role, as is the case for amorphous silica surfaces, all-silica zeolite external surfaces, and the internal walls of mesoporous materials.

Introduction

Silicas and silica-based materials are of paramount relevance for chromatography, adsorption, and metal–supported catalysis.[1–3] In all these cases, it is the silica surface rather than the bulk features that plays a key role in defining the behavior of the material. The silica surface features are dominated by the concentration, distribution and nature of hydroxyl groups, Si−OH.[4] Since long ago[5] it was established that a surface Si atom of an amorphous or crystalline silica can be bound to one or two OH surface groups, giving rise to silanols (≡Si−OH) and geminals (=Si−$(OH)_2$) terminations. Whereas the two OH groups of a geminal site are not mutually interacting via H-bonding[6] they, as well as the isolated silanols, when present in large amount on a silica surface, interact to each other via hydrogen bond. Thermal treatment of a silica sample at progressively high temperature will cause H-bonding pairs to condense by forming a siloxane bond Si−O−Si with the water removal. Further iteration of this process will bring about a silica surface sporting almost only isolated silanol groups. Nuclear spin cross polarization dynamics spectroscopy[7] as well as infrared and Raman spectroscopy,[5,8] together with analytical techniques,[9] have been adopted to investigate hydroxyls features on silica surfaces. However, due to the complexity of the hydrogen bond patterns at the surface these techniques are unable to provide structural features and atomic-resolution dynamics of the surface silanols. Recently, the great improvement in ab initio periodic programs has allowed the simulation of silica surfaces models either free[10] and interacting with water,[11–13] ammonia[14] and glycine.[15] Less accurate but faster techniques than the ab initio ones, such as classical molecular mechanics (MM) and molecular dynamics (MD), would be ideal for providing detailed interfacial properties of silica. The tradeoff is some loss in the quality of the results,

* Corresponding author. E-mail: piero.ugliengo@unito.it.
[†] University of Modena and Reggio Emilia.
[‡] University of Torino.

(1) Scott, R. P. W. *Silica Gel and Bonded Phases*; John Wiley & Sons: Chichester, U.K., 1993.
(2) Mull, D.; Sorsch, T.; Moccio, S.; Baumann, F.; Evas-Lutterodt, K.; Timp, G. *Nature* **1999**, 399.
(3) Nawrocki, J. *J. Chromatogr.* **1997**, *779*, 29.
(4) Iler, R. K. *The Chemistry of Silica*; Wiley-Interscience: New York, 1979.
(5) Knozinger, H. In *The Hydrogen Bond*; Schuster, P., Zundel, G.,Sandorfy, C., Eds.; North-Holland: Amsterdam, 1976; Vol. III; pp 1263.
(6) Ferrari, A. M.; Ugliengo, P.; Garrone, E. *J. Phys. Chem.* **1993**, *97*, 2671.
(7) Chuang, I.; Maciel, G. E. *J. Am. Chem. Soc.* **1996**, *118*, 401.
(8) Anedda, A.; Carbonaro, C. M.; Clemente, F.; Corpino, R.; Ricci, P. C. *J. Phys. Chem. B* **2003**, *107*, 13661.
(9) Mikhail, R. S.; Robens, E. *Microstructure and Thermal Analysis of Solid Surfaces*; John Wiley & Sons: New York, 1983.
(10) Civalleri, B.; Casassa, S.; Garrone, E.; Pisani, C.; Ugliengo, P. *J. Phys. Chem. B* **1999**, *103*, 2165.
(11) Rignanese, G.-M.; Charlier, J.-C.; Gonze, X. *Phys. Chem. Chem. Phys.* **2004**, *6*, 1920.
(12) Yang, J.; Meng, S.; Xu, L.; Wang, E. G. *Phys. Rev. Lett.* **2005**, *92*, 14102.
(13) Yang, J.; Wang, E. G. *Phys. Rev. B* **2006**, *73*, 035406.
(14) Civalleri, B.; Ugliengo, P. *J. Phys. Chem. B* **2000**, *104*, 9491.
(15) Rimola, A.; Sodupe, M.; Tosoni, S.; Civalleri, B.; Ugliengo, P. *Langmuir* **2006**, *22*, 6593.

10.1021/cm703437y CCC: $40.75
Published on Web 03/13/2008

particularly when rather weak intermolecular interactions are relevant, as is the case of hydrogen bonds between the surface silica hydroxyls. Until now, a number of efficient interatomic potentials for silica polymorphs bulk have been derived, both within the rigid ion scheme[16] and with the shell-ion model potential.[17,18] More recent and accurate potentials for simulating the features of silica bulk have also appeared.[19,20] Much less work was devoted to the development of reliable force fields for simulating not only the bulk, but also the silica surface features. The most widely adopted force field in that respect[21,22] poorly predicts OH vibrational frequencies, hydrogen bond geometries, and energies of interaction for the silica surfaces. More recently, interesting attempts to model reactivity of silica materials with water were carried out by means of new force fields,[23,24] none of these being meant to accurately model the H-bonding features (structural, energetic, and vibrational) occurring between surface silanols. Traditionally, force field parameters were derived from experimental data, using crystal structures, IR spectra and elastic properties (the classical case of α-quartz, for instance).[25] This approach suffers of one serious drawback in the present context: as mentioned earlier the lack of accurate experimental data about the silica surface physicochemical properties hampers a robust fit between computed and experimental data to be carried out. Alternatively, one can resort to ab initio parametrized interatomic potential models, usually derived by fitting the potential energy surface of a gas phase cluster, as proposed for the widely used bulk silica force fields.[17,18] More recently, a different strategy has been proposed by Tangey and Scandolo for silica bulk material[19] and by some of us for bulk hydroxyapatite.[26] Both works perform the fitting using results derived from a full ab initio periodic calculation on crystalline or structural models of amorphous materials. Following this approach we proposed a new shell-ion model potential for bulk hydroxyapatite $Ca_5(PO_4)_3(OH)$ from B3LYP periodic calculations, which showed to be excellent also to study other phosphates and a variety of hydroxyapatite surfaces.[27] The adoption of the B3LYP functional also ensured a high accuracy of the results, usually far better than pure GGA functional as far as hydrogen bond features are concerned.[28] In recent years, we showed that B3LYP used with reasonably flexible Gaussian basis sets and within the periodic boundary condition approach as encoded in the CRYSTAL06 code[29] gave very good results for OH vibrational feature occurring at the surface of edingtonite material.[10,30] Also, hydrogen bond features of the same surface in interaction with NH_3 were computed to be in excellent agreement with experiment.[14]

The same approach has been followed here to derive a new partial charge shell-ion model potential (FFSiOH), which is able to cope with the detailed features of hydroxylated silica surfaces.

Computational Details

All ab initio calculations have been carried out in a periodic fashion by the CRYSTAL06 program.[29] This code implements the Hartree–Fock and Kohn–Sham self-consistent field method for the study of periodic systems[31] and, in the present version, it allows to perform full geometry optimization[32] (atomic positions and lattice parameters), as well as to compute the phonon spectrum at Γ point of molecules, slab and crystals.[33,34] More technical details can be found in previous publications.[27,28,35] The tolerances for geometry optimization convergence have been set to the default values[29] and the Coulomb-exchange screening tolerances were set to (6 6 6 6 12) for all examined systems. Convergence on energy was set to 1×10^{-10} Hartree for frequency calculations and the displacement for computing the numerical energy second derivative set to the default value of 0.003 Å. An all-electron Gaussian basis set has been used with Si atom described by the standard 6–21G(d); oxygen and hydrogen were represented with a 6–31G(d,p) basis set with the most diffuse shell exponents α_{sp} and polarization α_d of 0.2742 $bohr^{-2}$ and 0.538 $bohr^{-2}$ and 0.1613 $bohr^{-2}$ and 1.1 $bohr^{-2}$, respectively. The B3LYP Hamiltonian - Becke's three-parameter (B3) hybrid exchange functional[36] in combination with the gradient-corrected correlation functional of Lee, Yang, and Parr[37] has been adopted for all calculations, as it is known to perform well, especially in solid state calculations.[38] In the DFT implementation, the exchange-correlation contribution is the result of a numerical integration of the electron density and its gradient, performed over a grid of points. CRYSTAL06 uses the Gauss-Legendre quadrature and Lebedev schemes to generate angular and radial points of the grid, respectively and a pruned grid of 75 radial points and 5 subinterval with a maximum of 974 angular points (75, 974) was used in this work, which ensures a good compromise between accuracy and cost of calculation, for geometry optimization and vibrational frequencies.[33,35] The Hamiltonian matrix has been diagonalized in a number of reciprocal lattice *k*-points,[39] i.e., 13

(16) Beest, B. W. H. v.; Kramer, G. J.; Santen, R. A. v. *Phys. Rev. Lett.* **1990**, *64*, 1955.
(17) de Boer, K.; Jansen, A. P. J.; van Santen, R. A. *Chem. Phys. Lett.* **1994**, *223*, 46.
(18) Sierka, M.; Sauer, J. *Faraday Discuss.* **1997**, *106*, 41.
(19) Tangney, P.; Scandolo, S. *J. Chem. Phys.* **2002**, *117*, 8898.
(20) Liang, Y.; Miranda, C. R.; Scandolo, S. *J. Chem. Phys.* **2006**, *125*, 194524.
(21) Feuston, B. P.; Garofalini, S. H. *J. Phys. Chem.* **1990**, *94*, 5351.
(22) de Leeuw, N. H.; Higgins, F. M.; Parker, S. C. *J. Phys. Chem. B* **1999**, *103*, 1270.
(23) Duin, A. C. T. v.; Strachan, A.; Stewman, S.; Zhang, Q.; Xu, X.; Goddard III, W. A. *J. Phys. Chem. A* **2003**, *107*, 3803.
(24) Hassanali, A. A.; Singer, S. J. *J. Phys. Chem. B* **2007**, *111*, 11181.
(25) Bush, T. S.; Gale, J. D.; Catlow, C. R. A.; Battle, P. D. *J. Mater. Chem.* **1994**, *4*, 831.
(26) Pedone, A.; Corno, M.; Civalleri, B.; Malavasi, G.; Menziani, M. C.; Segre, U.; Ugliengo, P. *J. Mater. Chem.* **2007**, *17*, 2061.
(27) Corno, M.; Orlando, R.; Civalleri, B.; Ugliengo, P. *Eur. J. Miner.* **2007**, *19*, 757.
(28) Ugliengo, P.; Pascale, F.; Mérawa, M.; Labéguerie, P.; Tosoni, S.; Dovesi, R. *J. Phys. Chem. B.* **2004**, *108*, 13632.
(29) Dovesi, R.; Saunders, V. R.; Roetti, C.; Orlando, R.; Zicovich-Wilson, C. M.; Pascale, F.; Civalleri, B.; Doll, K.; Harrison, N. M.; Bush, I. J.; D'Arco, P.; Llunell, M. *CRYSTAL06 User's Manual*; University of Turin: Torino, Italy, 2006; http://www.crystal.unito.it.
(30) Tosoni, S.; Pascale, F.; Ugliengo, P.; Orlando, R.; Saunders, V. R.; Dovesi, R. *Mol. Phys.* **2005**, *103*, 2549.
(31) Pisani, C.; Dovesi, R.; Roetti, C. Hartree-Fock ab-initio treatment of crystalline systems. In *Lecture Notes in Chemistry*; Springer: Berlin, 1988; Vol. 48.
(32) Civalleri, B.; D'Arco, P.; Orlando, R.; Saunders, V. R.; Dovesi, R. *Chem. Phys. Lett.* **2001**, *348*, 131.
(33) Pascale, F.; Zicovich-Wilson, C. M.; Lopez Gejo, F.; Civalleri, B.; Orlando, R.; Dovesi, R. *J. Comput. Chem.* **2004**, *25*, 888.
(34) Zicovich-Wilson, C. M.; Pascale, F.; Roetti, C.; Saunders, V. R.; Orlando, R.; Dovesi, R. *J. Comput. Chem.* **2004**, *25*, 1873.
(35) Prencipe, M.; Pascale, F.; Zicovich-Wilson, C. M.; Saunders, V. R.; Orlando, R.; Dovesi, R. *Phys. Chem. Miner.* **2004**, *31*, 1.
(36) Becke, A. D. *J. Chem. Phys.* **1993**, *98*, 5648.
(37) Lee, C.; Yang, W.; Parr, R. G. *Phys. Rev. B.* **1988**, *37*, 785.
(38) Cora', F.; Alfredsson, M.; Mallia, G.; Middlemiss, D. S.; Mackrodt, W. C.; Dovesi, R.; Orlando, R. *Struct. Bonding (Berlin)* **2004**, *113*, 171.
(39) Monkhorst, H. J.; Pack, J. D. *Phys. Rev. B.* **1976**, *8*, 5188.

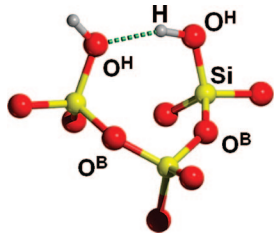

Figure 1. Atom types definition of the FFSiOH force-field.

(α-quartz, $P3_12_1$), 18 (α-cristobalite, $P4_12_12$), 8 (α-tridymite, $C222_1$), 75 stishovite ($P4_2/mnm$), 13 (chabazite, $R\bar{3}m$), 18 (edingtonite, $P\bar{4}$), and 3 (faujasite, $Fd\bar{3}m$), respectively. For all hydroxylated surfaces considered in the present work (vide infra) 13 reciprocal lattice *k*-points were used without symmetry constraints ($P1$ symmetry) but for the (010) face of the α-quartz for which 18 *k*-points within $P2_11$ symmetry. For chabazite and sodalite in which a Si atoms was replaced by four hydrogen atoms resulting in a single hydrogarnet defect $(OH)_4$ group per unit cell, the symmetry was reduced to $P1$ with 8 and 14 reciprocal lattice *k*-points being used, for chabazite and sodalite, respectively.

Molecular mechanics calculations as well as fitting procedure to define the FFSiOH parameters have been run by the GULP program, version 3.1.[40,41] Details about the fitting procedure are described in the next paragraph.

Adopted Classical Force-Field

The functional forms of the energy terms used by the new FFSiOH force-field are given in eq 1:

$$U = \sum_i \sum_{j>i} \frac{q_i q_j}{r} + \frac{1}{2}\sum_O k^O_{C-S}\left(r^O_S - r^O_C\right)^2 + \sum_a \left[A_a \exp(-r/\rho_a) - \frac{C_a}{r^6}\right] + \sum_b D_b\left[(1-\exp(-a_b(r-r_b)))^2 - 1\right] + \sum_{\text{three-body}}^{O-H\cdots O} \left(\frac{A}{r^{12}_{OO}} - \frac{B}{r^{10}_{OO}}\right)\cos^4\theta_{OHO} \quad (1)$$

Figure 1 shows the atom types definition: different ion types are assumed for the bridging ≡Si−O^B−Si≡ oxygen and the hydroxyl oxygen ≡Si−O^H−H and different short-range parameters are fitted for their mutual interaction.

The Born model assumes that ions interact via long-range electrostatic forces and short-range forces, which are described here as the combination of the electrostatic energy with the Buckingham potential (*a* stands for Si−O^B, O^B−O^B, O^B−O^H, O^H−O^H pairs, respectively) and a Morse potential acting between pairs *b* = Si−O^H, O^H−H, and H−bonds between OH···O^H and OH···O^B. The electronic polarizability of the ions is included via the shell-ion model potential of Dick and Overhauser,[42] in which each polarizable ion (here only the oxygen atoms) is represented by a core and a massless shell connected by a spring. The last term is a specific three-body potential for H-bonds, where θ is the angle characterizing the H-bond atomic sequence O−H···O. When θ > 90°, the energy angular term is that shown in eq (1), whereas it is set to zero when θ < 90°. The symbol r_{OO} is the distance between the two O atoms defining the O−H···O sequence. It is worth to mention that the hydrogen three-body term has been added at the end of the parametrization for dealing with strong H-bond interactions that we found in the hydrogarnet defects during the validation of the FFSiOH (see results). This is also the reason why the attractive term was set to zero and the final form is repulsive. Therefore, removing this term would lead to too short H-bond in high interacting systems like in the hydrogarnet defects but it does not affect the results obtained for all the simulated silica surfaces. The final form of the FFSiOH potential is the result of many trials using a variety of potential energy terms. The published ones have been judged as the best compromise on the base of our previous experience in developing force-fields. However, we are aware that different choices could give similar results once a proper calibration of parameters is achieved.

Fitting Strategy

To derive the FFSiOH parameters, we have selected the bulk as well as the (100) and (001) hydroxylated surfaces of α-cristobalite as training systems. The first step was to derive parameters apt to correctly model OH-free bulk silica materials, and the B3LYP structure and phonons of α-cristobalite were used as a reference set for this purpose. In a second step, the previously derived set of parameters was extended to model hydroxylated surface features using the B3LYP geometries and harmonic frequencies of α-cristobalite (001) and (100) surfaces.

The hydroxylated surfaces have been defined within the slab model in which a slab of a given thickness was cut out from the corresponding optimized bulk structure and the dangling bonds transformed in surface OH groups. Both faces (top and bottom) of the considered slabs were hydroxylated without imposing any symmetry constraints. Full B3LYP geometry optimization of both unit-cell size and internal coordinates was performed for the bulk and the two slabs. The optimized slabs thickness were 10 Å and 18 Å for the (100) and (001) faces, respectively and their main geometrical features are shown in Figure 2. On the optimized structures, full B3LYP harmonic frequencies were computed using the numerical conditions reported in the Computational details.

The de Boer et al.[17] set of parameters was adopted as the initial guess of the FFSiOH parameters (keeping only the Si charge fixed to its original value). Unlike previous shell model force-fields,[18] partial charges have been used. The silicon charge was fixed to Boer et al.[17] original value while the total charges for bridging oxygen and for the OH group have been refitted imposing the condition $q(O^B) = q(Si)/2$ and $q(OH) = q(Si)/4$. Missing parameters for atomic types not present in the de Boer et al.[17] force field were guessed on an intuitive base and subsequently refined during the fitting procedure. Figure 2 (top) shows the (001) α-cristobalite surface, which sports pairs of hydrogen-bonded geminal silanols. The unit cell contains one OH group involved in a rather short hydrogen bond (H···O = 1.697

(40) Gale, J. D. *J. Chem. Soc., Faraday Trans.* **1997**, *93*, 629.
(41) Gale, J. D.; Rohl, A. L. *Mol. Simul.* **2003**, *29*, 291.
(42) Dick, B. G.; Overhauser, A. W. *Phys. Rev.* **1958**, *112*, 90.

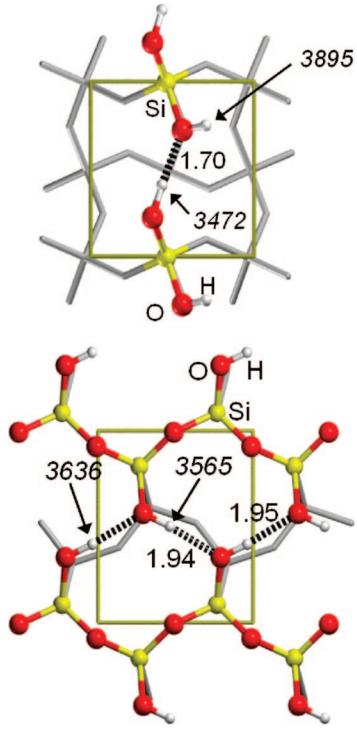

Figure 2. B3LYP optimized unit-cell structure of the (001) (top) and (100) (bottom) faces of hydroxylated α-cristobalite. H···O hydrogen bond distances in Å (as dotted lines), vibrational OH stretching frequencies (in italic) in cm^{-1}.

Å) with an associated OH streching frequency of 3472 cm^{-1}. The second OH group, not engaged in H-bonding, vibrates at much higher frequency (3895 cm^{-1}). Figure 2 (bottom) shows the (100) α-cristobalite surface envisaging chains of hydrogen bonded geminal groups that extent across the whole surface. The unit cell contains two almost equivalent H-bonded OH groups (H···O distances of 1.938 and 1.953 Å, respectively) with associated stretching frequencies of 3565 and 3636 cm^{-1}, respectively. The simultaneous conventional fitting scheme included in the GULP package[41] has been adopted. In this method, gradients and properties are calculated and the potential parameters and shell ion positions are varied so as to minimize the error in these quantities through a least-squares procedure.

The H-bond between O^H−H groups and bridging O^B oxygen is encoded by a Morse function between H and $O^{H/B}$ atoms not directly bound via a covalent bond. To ensure a well balanced parametrization and a robustness in the fit, different weights were given to different types of data. There are several criteria that can be used for their choice. First, when fitting on experimental data, the weighting factor should be inversely proportional to the uncertainty in the measured value, a fact which does not apply when fitting to theoretical values as in the present case. Second, the weight factor should be inversely proportional to the magnitude squared of the corresponding observable. This ensures that all values are fitted on an equal footing, regardless of units. Therefore, based on the second criteria the B3LYP harmonic frequencies were weighted with a factor of 1×10^{-3} since their number is ca. 3 orders of magnitude larger than the number of corresponding energy gradient components which were weighted 1.0. This results in parameters which give both good structures and harmonic vibrational frequencies. A complete GULP input for the α-cristobalite (100) surface is provided in the Supporting Information. The final FFSiOH parameters are listed in Table 1. Note that there is no dispersion interaction ($C_a = 0$) for the Buckingham potential, since the attractive interactions are subsumed by the electrostatic interactions.

Table 1. FFSiOH Shell-Ion Model Potentials Parameters Definition (see the Supporting Information for a complete GULP input)[a]

Buckingham Potential Parameters			
	A (eV)	ρ (Å)	C (eV Å^6)
O^B_s−O^B_s	15039.909	0.227708	
Si−O^B_s	8166.2632	0.193884	
O^H_s−O^H_s	1688.1482	0.292545	
O^H_s−O^B_s	6768.7644	0.245932	
Morse Potential Parameters			
	D (eV)	a (Å^{-1})	r_0 (Å)
Si−O^H_s	0.04589720	2.6598	2.33921
H−O^H_s	0.00935906	3.2461	1.76617
Morse ×12 Potential Parameters			
	D (eV)	a (Å^{-1})	r_0 (Å)
H···O^H_S[b]	0.11097337	1.0230	2.33429
H···O^B_S[c]	0.00643903	1.8794	3.17953
Three-Body Hydrogen Bond Potential Parameters			
	A (eV/Å^{12})	B (eV Å^{10})	
O^H_S−H···O^H_S	3653.260		

[a] The shell model is for oxygen only with parameters $q_c(O^B) = 1.919810$, $q_s(O^B) = -3.281110$, $k_{c-s} = 256.71027$, $q_c(O^H) = 1.429114$, $q_s(O^H) = -2.767837$, $k_{c-s} = 160.84247$. Core charges for Si and H are $q_c(Si) = 2.7226$ and $q_c(H) = 0.658073$. Atom types are shown in Figure 1. [b] Cut-off of 3.0 Å. [c] Cut-off of 4.0 Å.

Results and Discussion

Testing the FFSiOH Force Field for Nonhydroxylated Systems. In order to prove the predictive power of the FFSiOH the following strategy has been adopted. First, the FFSiOH was used to predict structures, relative energies and vibrational frequencies at harmonic level of bulk silica materials, either dense silica polymorph (α-quartz, α-cristobalite, α-tridymite, and Stishovite) and microporous (chabazite, edingtonite, and faujasite).

Relevant structural features of the FFSiOH predicted structures are reported in Tables 2 and 3, for the dense and microporous materials, respectively, and compared with experimental and B3LYP data. B3LYP cell parameters for α-cristobalite are reproduced by the force field within 0.7% deviation. Slightly higher differences are computed for the other polymorphs. Despite the well-known Si−O bond length overestimation by B3LYP calculations,[18,43] the FFSiOH gives results in good agreement with experimental data. The most delicate quantity is the Si−O−Si angle, due to its extreme flexibility, as shown by ab initio calculations.[43] Its value is underestimated by 4 and 3° for α-quartz and α-cristobalite while larger variations of about 5, 26, and 21° compared to experimental data are computed for α-tridymite.

(43) Bar, M. R.; Sauer, J. *Chem. Phys. Lett.* **1994**, *226*, 405.

Table 2. Experimental, (B3LYP) and [FFSiOH] Unit-Cell Parameters (*a*, *b*, *c*), Cell Volume (*V*), Average Si−O Bond Length (<Si−O>) and Si−O−Si Bond Angle (Φ) for α-Quartz, α-Cristobalite, α-Tridymite, and Stishovite (distances in Å, angles in deg, volume in Å^3)

	α-quartz[a] $P3_12_1$	α-cristobalite[b] $P4_12_12$	α-tridymite[c] $C222_1$	Stishovite[d] $P4_2/mnm$
a	4.914	4.971	8.756	4.177
	(4.971)	(5.024)	(8.869)	(4.223)
	[4.911]	[5.011]	[8.705]	[4.274]
b			5.024	
			(4.968)	
			[5.000]	
c	5.406	6.928	8.213	2.660
	(5.467)	(6.989)	(8.267)	(2.699)
	[5.404]	[6.940]	[8.534]	[2.654]
V	113.1	171.2	361.6	46.4
	(117.0)	(176.4)	(364.0)	(48.1)
	[112.9]	[174.2]	[371.5]	[48.5]
<Si−O>	1.610	1.603	1.559	1.755 1.808
	(1.632)	(1.630)	(1.626)	(1.777 1.831)
	[1.633]	[1.630]	[1.628]	[1.770 1.851]
Φ	144	147	180 171 161	131 99
	(143)	(145)	(174 143 142)	(131 99)
	[140]	[144]	[175 145 140]	[132 97]

[a] Experimental data from ref 66. [b] Experimental data from ref 67. [c] Experimental data from ref 68. [d] Experimental data from ref 69.

Table 3. Experimental, (B3LYP) and [FFSiOH] Unit-Cell Parameters (*a*, *b*, *c*), Cell Volume (*V*), Average Si−O Bond Length (<Si−O>) and Si−O−Si Bond Angle (Φ) for All-Silica Chabazite, Edingtonite, and Faujasite (distances in Å, angles in deg, volume in Å^3)

	chabazite[a] $R3\bar{m}$	edingtonite $P\bar{4}2_12$	faujasite[b] $Fd3m$
a	9.229		24.26
	(9.360)	(6.955)	(24.58)
	[9.388]	[6.959]	[24.63]
c			
		(6.436)	
		[6.401]	
V	745		14278
	(811)	(311)	(14848)
	[817]	[310]	[14938]
<Si−O>	1.599		1.606
	(1.628)	(1.633)	(1.631)
	[1.627]	[1.633]	[1.630]
Φ	149 149		138 141 146 149
	(149 150)	(141 138 179)	(139 141 144 148)
	[150 152]	[140 138 179]	[140 143 144 147]

[a] Experimental data from ref 70. [b] Experimental data from ref 71.

Interestingly, FFSiOH prediction of the Stishovite structure (silicon is 6-fold coordinated) is surprisingly good: this is due to the lack of a three O^B-Si-O^B body term in FFSiOH, which is needed to reproduce the tetrahedral coordination of silicon in low pressure polymorphs[18,44,45] when formal charges are used but which would had hampered the octahedral Si-coordination to be modeled correctly. Almost perfect agreement with B3LYP results was found for microporous polymorphs structures (see Table 3), with deviations below 0.5% on cell parameters. The deviation on the Si−O−Si bending angles is below 2° and demonstrates that the FFSiOH force-field is able to reproduce a wide range of Si−O−Si bending angles present in the considered silica polymorphs.

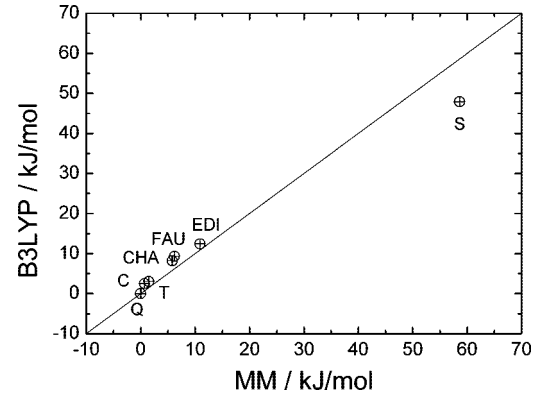

Figure 3. Correlations between B3LYP and MM FFSiOH relative stabilities at 298 K for the bulk structures for α-crystobalite (C), α-tridymite (T), chabazite (CHA), edingtonite (EDI), faujasite (FAU), and Stishovite with respect to the α-quartz (Q) (set as zero energy).

A severe test for the derived force field is the prediction of the relative stability of the silica polymorphs compared to the most stable α-quartz phase. The lattice energy minimization shows that α-cristobalite, α- tridymite, Stishovite, chabazite, edingtonite and faujasite are 0.71, 1.5, 58.6, 5.8, 10.9, and 6.9 kJ/mol less stable than α-quartz, in reasonable agreement with B3LYP data of 2.5, 3.0, 47.9, 8.2, 12.4, and 9.3 kJ/mol (all computed at 298 K). Figure 3 shows the correlation between the B3LYP and FFSiOH relative phase stabilities. Experimental data of 2.6, 2.9, 11.4, and 13.6 kJ/mol measured at 298 K[46,47] are available for α-cristobalite, α-tridymite, chabazite, and faujasite, respectively, in good agreement with the FFSiOH predictions.

Figure 4 shows the correlation between the B3LYP and FFSiOH vibrational frequencies of the dense silica polymorphs and of the microporous ones. Very good agreement has been achieved for all cases, the average difference being of 14, 10, 20, 18, 16, and 15 cm^{-1} for α-quartz, α-cristobalite, α-tridymite, chabazite, edingtonite and faujasite, respectively. It is worth of note that the B3LYP method with the present basis set gives vibrational frequencies that are in excellent agreement with those accurately determined for quartz,[34] cristobalite, and tridymite,[48] which means that the same kind of agreement with experiment is foreseen for FFSiOH force field.

The reliability, accuracy, and transferability of FFSiOH have also been tested by comparing the calculated vibrational density of states (VDOS) of vitreous silica v-SiO_2 with the experimental one[49] from inelastic neutron scattering measurements (see Figure 5). The structure of vitreous silica obtained by melt-quench process using the rigid ionic model[50,51] has been reoptimized at constant pressure (0 GPa) and the VDOS has been calculated at the Γ point with the

(44) Sanders, M. J.; Leslie, M.; Catlow, C. R. A. *J. Chem. Soc., Chem. Commun.* **1984**, 1271.
(45) Tilocca, A.; de Leeuw, N. H.; Cormack, A. N. *Phys. Rev. B* **2006**, *73*, 104209.
(46) Saxena, S. K.; Chatterjee, N.; Fei, Y.; Shen, G. *Thermodynamic Data on Oxides and Silicates*; Springer-Verlag: Berlin, 1993.
(47) Piccione, P. M.; Laberty, C.; Yang, S.; Camblor, M. A.; Navrotsky, A.; Davis, M. E. *J. Phys. Chem. B* **2000**, *104*, 10001.
(48) Musso, F.; Corno, M.; Ugliengo, P. In preparation.
(49) Arai, M.; Hannon, A. C.; Taylor, A. D.; Otomo, T.; Wright, A. C.; Sinclair, R. N.; Price, D. L. *Trans. Am. Crystallogr. Assoc.* **1991**, *27*, 113.
(50) Pedone, A.; Malavasi, G.; Menziani, M. C.; Cormack, A. N.; Segre, U. *J. Phys. Chem. B* **2006**, *110*, 11780.
(51) Pedone, A.; Malavasi, G.; Cormack, A. N.; Segre, U.; Menziani, M. C. *Chem. Mater.* **2007**, *19*, 3144.

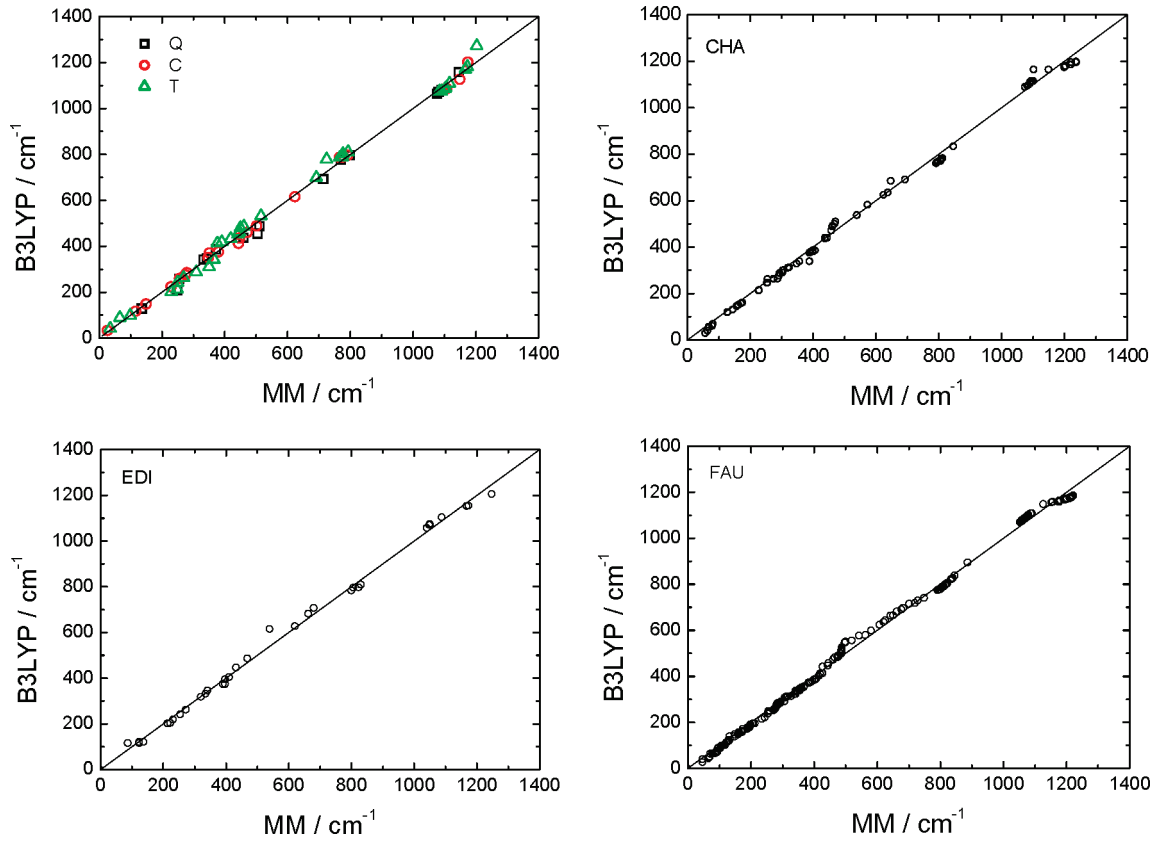

Figure 4. Correlations between B3LYP and MM FFSiOH full set of harmonic vibrational frequencies for the bulk structures of: (top left) α-quartz (Q), α-crystobalite (C) and α-tridymite (T); (top right) chabazite (CHA); (bottom left) edingtonite (EDI); (bottom right) faujasite (FAU).

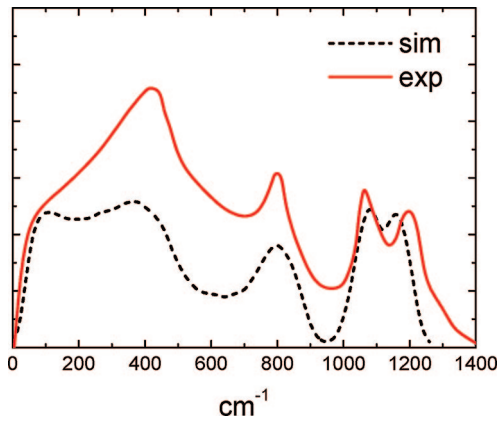

Figure 5. Experimental[49] (continuous line) and MM FFSiOH (dashed line) vibrational density of states of vitreous silica v-SiO_2.

FFSiOH force-field. Two bands are clearly seen in the spectrum, in the 0–600 cm^{-1} region and the 600–1300 cm^{-1} one. The highest band has two pronounced peaks related to the longitudinal and transverse stretching vibrations of the SiO_4 units while the band at 800 cm^{-1} is related to the Si−O−Si bending mode.[52–54] The structure of the lowest band is rather intermingled because of the overlap between bands. Structural disorder in glasses causes a broadening of the sharp band edges of crystals which become band tails.

The main features of the VDOS shown in Figure 5 (a wide lower frequency band between 0 and 600 cm^{-1} and the narrow peaks at 800 and 1100–1200 cm^{-1} separated by a gap of 200 cm^{-1}) are similar to those obtained for the different structural silica polymorphs reported above.

The FFSiOH VDOS fits the experimental curve with an accuracy never reached before with other models potential. Taraskin et al.[55] simulated the VDOS of v-SiO_2 by using the van Beest[16] and the Tsuneyuki[56] potential which are rigid ionic models fitted on quantum mechanical and experimental observables. The deficiency of the Tsuneyuki potential results in a shift of the spectrum in the high-frequency region to lower frequencies by ∼100 cm^{-1} with respect to the experimental VDOS. Neither the van Beest nor the Tsuneyuki potential can reproduce a pronounced peak in the intermediate frequency region at 400 cm^{-1} found in inelastic neutron scattering measurements.[46] This may be due to a deficiency of the potentials which describe the bending modes of SiO_4 structural units. Remarkably, the majority of phenomenological and semiphenomenological potentials to date share this deficiency. Notable exceptions are the phenomenological three-body interatomic potentials by Feuston-Garofalini[21] and the Vashista potential,[57] which despite predicting a peak around 350 cm^{-1} do not reproduce the shape of the high-frequency band.

Testing the FFSiOH Force Field for Hydroxylated Systems. As a second step, a number of silica based systems inclusive of surface OH groups have been considered. Let

(52) Bell, R. J.; Dean, P. *Discuss. Faraday Soc.* **1970**, *50*, 55.
(53) Laughlin, R. B.; Joannopoulos, J. D. *Phys. Rev. B* **1977**, *16*, 2942.
(54) Handke, M.; Mozgawa, W. *J. Mol. Struct.* **1995**, *348*, 341.
(55) Taraskin, S. N.; Elliott, S. R. *Phys. Rev. B* **1997**, *56*, 8605.
(56) Tsuneyuki, S.; Tsukada, M.; Aoki, H.; Matsui, Y. *Phys. Rev. Lett.* **1988**, *61*, 869.
(57) Jin, W.; Vashishta, P.; Kalia, R. K.; Rino, J. P. *Phys. Rev. B* **1993**, *48*, 9359.

Table 4. Unit-Cell Parameters (a, b, γ), Cell Surface Area (A), Average Si−OH and O−H bond lengths (<Si−OH>, <O−H>), Average Si−O−H Bond Angle (<Ω>), H···O Hydrogen Bond Distance, and O−H Stretching Frequencies (ν(OH)) of the (100) Surfaces for α-Quartz (Q(100)), α-Cristobalite (C(001)), and α-Tridymite (T(001)) Compared to B3LYP Data (distances in Å, angles in deg, area in Å^2, frequencies in cm^{-1})

	Q(100)		C(100)		T(100)	
<Ω>	B3LYP	MM	B3LYP	MM	B3LYP	MM
a	4.9669	4.901	5.140	5.128	5.080	5.075
b	5.4568	5.425	5.982	6.026	7.923	7.936
γ	88.8	88.6	90.0	90.0	90.0	90.0
A	27.10	26.58	30.7	30.9	40.3	40.3
<Si−OH>	1.640	1.642	1.643	1.640	1.640	1.635
<O–H>	0.975	0.976	0.979	0.977	0.970	0.970
	116.4	117.1	119.4	120.3	117.5	120.0
H···O	1.805	1.802	1.947	1.963	1.897	1.880
	2.223	2.181	1.949	1.963		
ν(OH)	3510	3531	3565	3570	3668	3665
	3573	3578	3569	3570	3687	3665
	3709	3705	3636	3617	3880	3896
	3877	3880	3638	3617	3888	3896

us start with results of Table 4 showing the FFSiOH predicted structure and harmonic OH stretching frequencies of the (100) hydroxylated surfaces of α-quartz, α-cristobalite and α-tridymite in comparison with the B3LYP values. Differences <0.7% have been computed for the cell parameters of the C(100) and T(100) surfaces, while differences of 1–2% resulted for the Q(100) surface, showing that the same accuracy for bulk structures is found for hydroxylated silica surfaces. Excellent agreement has been obtained for the Si−OH angle (<1°) and O−H bond lengths (<0.001 Å) in comparison with B3LYP data. The most important result is the reproduction of hydrogen bond features, as the agreement of the H···O distances at the surfaces is very good, the largest difference between FFSiOH and B3LYP data being of 0.07 Å for the T(100) surface. An even more stringent test is represented by the O−H harmonic stretching frequencies, as shown in Table 4. Average differences between FFSiOH and B3LYP frequencies of 8, 11, and 13 cm^{-1} have been computed for the hydroxyl groups at the Q(100), C(100), and T(100) surfaces, respectively.

Further checks of the ability of the FFSiOH in dealing with hydrogen bond features were carried out on a larger set of hydroxylated faces of the dense silica polymorphs, namely, the (001), (010), (100), (011), and (101) faces of α-quartz; the (001), (100), (101), and (110) faces of α-cristobalite; and the (001), (100), and (110) faces of α-tridymite. The detailed discussion of the B3LYP optimized structures is outside the scope of the present work and will be discussed elsewhere.[48] Main structural features are reported in Figure S1 of the Supporting Information. To increase the number of possible hydrogen bond topologies at the surface of silica materials the following systems were also considered: (i) hydroxylated (001) and (100) surfaces of edingtonite, envisaging isolated and H-bonded interacting silanols (structures EDI-IS and EDI-HB shows in Figure S2 of the Supporting Information); (ii) a slab model of amorphous silica envisaging a 13.7 × 14.0 Å cell with 7.2 OH/nm^2 which was fully relaxed at B3LYP level (Figure S3 of the Supporting Information) sporting, as a whole, 13 hydrogen

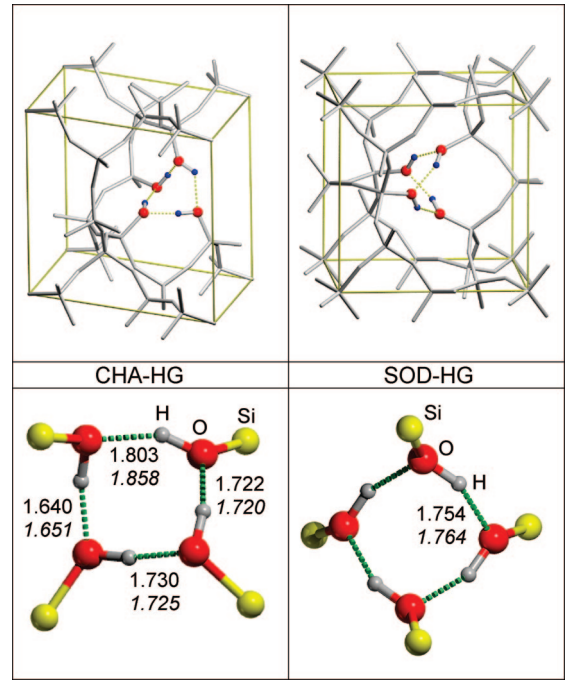

Figure 6. (Top) Unit cells of chabazite (CHA-HG) and sodalite (SOD-HG) hydrogarnet. The OH groups are highlighted as red and blue spheres; framework atoms as grey stick. (Bottom) Enlarged view of the B3LYP (italic) and FFSiOH intermolecular H···O intermolecular H-bond distances of the hydrogarnet; distances in Å.

bonds of different strength;[58] (iii) the hydrogarnet Si(OH)$_4$ defect in both chabazite and sodalite structures.[59] The adopted model for the amorphous silica surface sports a higher OH density than the one (4.5 OH/nm^2) usually accepted on the base of experimental evidence,[60] as the highest for an amorphous silica material. The reason is due to the way in which the surface was defined starting from a glassy cristobalite bulk structure which will be the subject of future publications.[61] For the present purpose of comparing B3LYP with FFSiOH structures and frequencies, working with a higher OH density does not affect the final results. The hydrogarnets are intriguing defects resulting from loss of Si atoms from the silica framework. The healing of the defective structure is provided by four OH groups hanging from the framework and undergoing hydrogen bond interactions whose strength is a function of the silica framework. Figure 6 shows the hydrogarnet in chabazite (CHA-HG) and sodalite (SOD-HG) frameworks. Four hydrogen bonds of different strength are computed for CHA-HG whereas a fully symmetrical defect resulted for SOD-HG. The comparison between B3LYP and FFSiOH of the H···O distances reveal a very good agreement for both defects, the largest deviation being 0.05 Å. The whole sets of B3LYP and FFSiOH H···O intermolecular distances and harmonic O−H vibrational stretching frequencies for all considered cases are compared in panels a and b in Figure 7, respectively. The correlation is excellent, (average deviation of 0.023 Å and 20 cm^{-1} for

(58) Ugliengo, P.; Bush, I. J.; Orlando, R.; Sodupe, M.; Musso, F. In preparation.
(59) Pascale, F.; Ugliengo, P.; Civalleri, B.; Orlando, R.; D'Arco, P.; Dovesi, R. *J. Chem. Phys.* **2002**, *117*, 5337.
(60) Zhuravlev, L. T. *Langmuir* **1997**, *3*, 316.
(61) Ugliengo, P.; Sodupe, M.; Musso, F.; Bush, I. J.; Orlando, R.; Dovesi, R. in preparation.

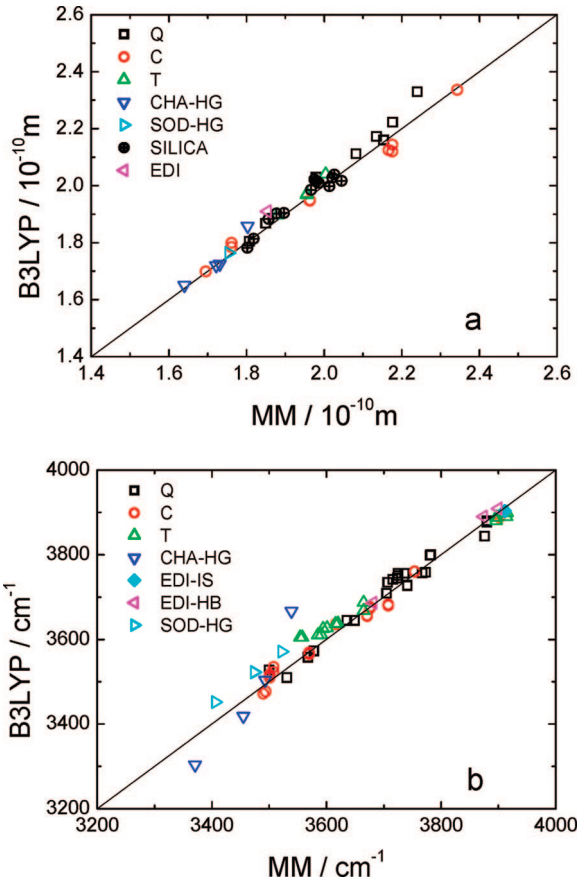

Figure 7. (a) Correlations between B3LYP and MM FFSiOH intermolecular H···O hydrogen bond distance for all crystal surfaces derived from α-quartz (Q), α-crystobalite (C), α-tridymite (T), chabazite (CHA-HG), and sodalite (SOD-HG) hydrogarnets, the isolated and H-bonded silanols of the edingtonite surfaces (EDI), and a model of amorphous silica surface with 7.2 OH groups per nm^2 (SILICA). (b) Correlations between B3LYP and MM FFSiOH harmonic O-H stretching frequency for all crystal surfaces derived from α-quartz (Q), α-crystobalite (C), α-tridymite (T), chabazite (CHA-HG), and sodalite (SOD-HG) hydrogarnets and for isolated (EDI-IS), and H-bonded silanols (EDI-HB) of the edingtonite surfaces.

OH and ν(OH), respectively) when considering that the H···O distance and the ν (OH) stretching span 0.8 Å and more than 600 cm^{-1}, respectively. The largest deviation is observed for the ν(OH) values associated to CHA-HG probably because hydrogen bond cooperativity in the ring is not properly taken into account by the FFSiOH.

The results discussed so far were obtained by using the B3LYP optimized geometry as a starting point for the FFSiOH geometry relaxation. To ensure that the FFSiOH was able to recover the B3LYP geometry also when starting from structures far away from the minima, a series of check calculations were carried out, as described in the following. For the (101) surface of cristobalite, the (100) and (101) of quartz and the (110) of tridymite as well as for both faces of the amorphous silica surface model, the optimum H-bond pattern was destroyed by allowing rotation of the OH groups around the Si−O bond by ± 40 degrees combined with variations in the Si−O−H angle, so to guarantee a rather deformed starting geometry for all considered cases. Reoptimization using the FFSiOH completely recovers the B3LYP H-bond pattern, showing that FFSiOH force field is accurate enough also far away from the minimum region to which it was parametrized. Larger variations in the considered

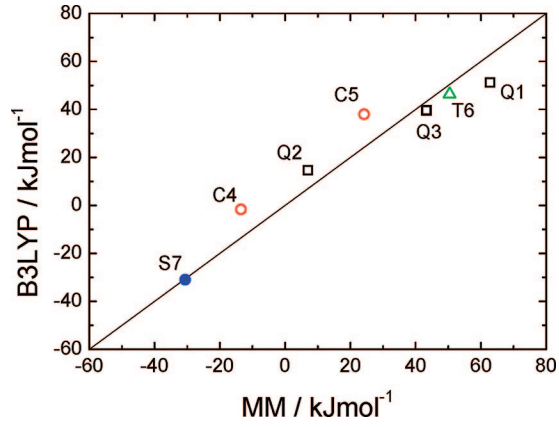

Figure 8. Correlation between B3LYP and MM FFSiOH relative energies for different hydroxylated surfaces and the hydrogarnet stability in CHA and SOD framework (see text for details).

variables, particularly for the amorphous silica surface model, will eventually bring the considered structures in different local minima, which are not, however, cross-checked by running new B3LYP calculations that would have been exceedingly expensive for the present purpose.

Testing the FFSiOH Force Field for H-Bond Energetics. FFSiOH has also been checked against B3LYP results for the ability to compute the thermodynamic stability of the hydroxylated faces derived from the dense silica polymorphs. Using the FFSiOH and B3LYP total energies per unit cell (without considering thermal corrections) the following solid state equilibria, that represent relative stability of different hydroxylated faces within the same silica polymorph, have been considered:

Q1: Q(001) ↔ Q(010)
Q2: Q(100) ↔ 1/2 Q(011) + 1/2 Q(001)
Q3: Q(101) ↔ 2 Q(011)
C4: C(001) ↔ 1/2 C(101) + 1/2 C(100)
C5: C(100) ↔ 2/7 C(110) + 3/7 C(101)
T6: T(100) ↔ 2 T(001)
S7: CHA-HG ↔ SOD-HG

Reaction S7 deals with the stability of the hydrogarnet defect in either chabazite or sodalite frameworks. Results are shown in Figure 8. Considering the rather simple form of the adopted force field and that energetic data were not included in the training set, the agreement is reasonable, with the average error of 7.5 kJ/mol.

Testing the FFSiOH Force Field against Experimental Data for Hydroxylated Surfaces. As reported in the introduction, it is very hard to assess the performance of FFSiOH force field with respect to experimental data. Two obstacles are relevant in that respect: (i) the geometry of the local environment around the OH groups at the surface of any silica based material is unknown; ii) the vibrational spectrum in the OH stretching region sports a very broad and featureless band because of the hydrogen bond interactions of variable strength.[5,62] A further difficulty is that the harmonic OH vibrational results cannot be compared straightforwardly with the experimental ones, because anharmonicity is relevant for the OH group. Our recent work in that

(62) Jeffrey, G. A. *An Introduction to Hydrogen Bonding*; Oxford University Press: New York, 1997.

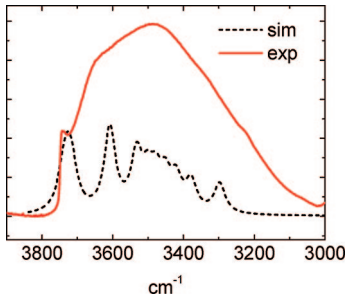

Figure 9. Comparison between B3LYP (dashed line) and experimental infrared spectra (continuous line) for α-cristobalite surface in the OH stretching region. The experimental spectrum[64] has been recorded on a microcrystalline powder outgassed at 150 °C to remove the adsorbed water. See text for details about the simulation of the B3LYP spectrum.

respect[14,28,30,59] showed that the anharmonic correction $\omega_e x_e$ to the OH harmonic stretching frequency is rather large and its value is a function of the hydrogen bond strength. As a check for the reliability of the B3LYP results, which in turn determine the quality of the FFSiOH, the infrared spectrum of the hydroxylated cristobalite surface in the OH stretching region has been simulated in a very simplified way. First, all the harmonic OH B3LYP stretching frequency values were scaled by the factor 0.958 resulting from the comparison of the B3LYP anharmonic frequency of 3742 cm^{-1} for the isolated OH group at the (001) edingtonite surface[10] and its harmonic counterpart of 3903 cm^{-1}. The B3LYP anharmonic value of 3742 cm^{-1} is extremely close to the experimental value of 3745 cm^{-1}, which is the fingerprint of the isolated silanol at the surface of almost all silica based materials,[5] giving credit to the adopted methodology.[14] Using the infrared intensities computed at B3LYP level[63] the B3LYP infrared spectrum is simulated by summing up the contributions of the OH stretching frequencies from the four considered α-cristobalite hydroxylated surfaces, i.e. the (001), (100), (101), and (110) ones. Each OH band has been broadened by means of a Lorentzian function, each 40 cm^{-1} width. Despite the roughness of this approach, as shown in Figure 9, the general agreement with the experimental spectrum recorded on a microcrystalline powder sample of α-cristobalite pretreated at 150 °C to remove the adsorbed water[64] is evident: the range of the bathochromic shift (about 600 cm^{-1}) suffered by the free OH frequency due to H-bond is well reproduced by the B3LYP method. Clearly, due to the larger variety of crystal faces present in the microcrystalline sample, one cannot expect the simulated B3LYP spectrum (derived from only four faces) to mimic all features of the experimental one. Because FFSiOH has been shown above to provide results very close to the B3LYP ones, it is expected to behave with similar predictive power in that respect.

Summary and Conclusions

A new force field, FFSiOH, based on a rather simple shell-ion model potential definition, whose parameters have been derived using exclusively periodic B3LYP calculation on α-cristobalite, has been proposed as a method to treat equally well the bulk and the surface features of silica based materials. It has been demonstrated that for bulk materials, FFSiOH can predict structure, energetic and vibrational features of both dense silica polymorphs and a selection of microporous all-silica materials with better overall quality of the most successful force fields of the literature.[16,18] At variance with the previous force fields, however, FFSiOH has been also extended to cope with the hydroxylated surfaces of silica based materials. Whereas these surfaces may also be OH free, this only occurs after very harsh treatment at high temperature. For the largest variety of silica materials, either crystalline or amorphous, the surface sports OH groups at various degree of coverage, giving rise to complex hydrogen bond networks which, in turn, determine the surface features of the material. This is relevant in many fundamental and technological aspects, in that SiO_2 is an ubiquitous material, for instance in microelectronics fiber optics technology, as a support for metal catalysts and in chromatography. In all these aspects, its surface features play a key role. Also internal defective OH groups in bulk materials, such as the hydrogarnet defects, have been considered. Due to the paucity of accurate experimental data for the silica surface features, FFSiOH results has been checked against B3LYP ones, these latter having shown in the past to be very accurate in predicting the relevant features of silica based materials. From the whole set of reported data (surfaces of α-quartz (5), α-cristobalite (4), α-tridymite (3), edingtonite (2), amorphous silica model (2), chabazite, and sodalite hydrogarnets) one can conclude that FFSiOH is capable to deal with the large variety of H-bonding interactions occurring on silica based materials with an unprecedented accuracy. Hydroxylated silica surfaces are rarely free from adsorbed water and experimentally only silica samples treated at temperature higher than 700 K are considered water free. These samples, however, when left to the action of moisture rapidly capture water at their surface. Therefore, it would be interesting to extend the FFSiOH force field to incorporate water molecules and their interaction with silica silanols, a task which is now in progress in our laboratory. It is believed that the adoption of FFSiOH in QM/MM schemes, as it is commonly done for instance in the QM-Pot scheme,[65] will improve the accuracy of the characteriza-

(63) Zicovich-Wilson, C. M.; Dovesi, R.; Saunders, V. R. *J. Chem. Phys.* **2001**, *115*, 9708.
(64) Fenoglio, I.; Ghiazza, M.; Ceschino, R.; Gillio, F.; Martra, G.; Fubini, B. The role of nature and structure of the surface sites in the biological response to silica particles. In *NATO Science Series II: Mathematics, Physics and Chemistry. Surface Chemistry in Biomedical and Environmental Science*; Blitz, J. P., Gun'ko, V. M., Eds.; Springer: New York, 2006; Vol. 228; pp 287.
(65) Eichler, U.; Kolmel, C. M.; Sauer, J. *J. Comput. Chem.* **1997**, *18*, 463.
(66) Smith, G.; Alexander, L. E. *Acta Crystallogr.* **1963**, *16*, 462.
(67) Pluth, J. J.; Smith, J. V.; Faber, J. J. *Appl. Phys.* **1985**, *57*, 1045.
(68) Kihara, K.; Matsumoto, T.; Imamura, M. *Z. Kristallogr.* **1986**, *117*, 27.
(69) Spackman, M. A.; Hill, R. J.; Gibbs, G. V. *Phys. Chem. Minerals* **1987**, *14*, 139.
(70) Diaz-Cabanaz, M.-J.; Barrett, P. A.; Camblor, M. A. *Chem. Commun.* **1988**, 1881.
(71) Hriljac, J. A.; Eddy, M. M.; Cheetham, A. K.; Donohue, J. A.; Ray, G. J. *J. Solid State Chem.* **1993**, *106*, 66.

tion of many complex phenomena occurring at the surface of silica based materials by means of purely computational methods.

Acknowledgment. Financial support from the Italian Ministry MIUR (Project COFIN2006, Prot. 2006032335_005) and from the Regione Piemonte (Bando ricerca scientifica Piemonte 2004, Settore: Nanotecnologie e nanoscienze, "Materiali nanostrutturati biocompatibili per applicazioni biomediche") is gratefully acknowledged. The Barcelona Supercomputing Center (http://www.bsc.es) is acknowledged for generous allowance of computer resources at *MareNostrum* (Project QCM-2007-1-0002, "Ab initio simulation of amorphous silica surface and its interaction with biological molecules"). G. Martra (Dip. Chimica IFM, Università di Torino, Italy) and J. Gale (Dep. Applied Chemistry, Curtin University of Technology, Perth, Western Australia) are acknowledged for providing, respectively, the IR spectrum of α-cristobalite and the GULP 3.3 prerelease and for fruitful discussion.

Supporting Information Available: Pictures of all considered systems and the GULP input file of the geometry optimization and frequency calculation of the (001) surface of cristobalite are available as Supporting Information (PDF). This information is available free of charge via the Internet at http://pubs.acs.org.

CM703437Y